

Library Copies
R.A. #73 2109

UNCLASSIFIED
~~CONFIDENTIAL~~

C.2

Copy 44
RM SL55F24

CLASSIFICATION CHANGED



~~CONFIDENTIAL~~

Authority *SC-STAR* Date *11-30-70*
V-8, No. 22 *Blom*

RESEARCH MEMORANDUM

12/22/7

for the

U. S. Air Force

FLIGHT DETERMINATION OF THE
LONGITUDINAL STABILITY AND CONTROL CHARACTERISTICS OF A
0.125-SCALE ROCKET-BOOSTED MODEL OF THE MCDONNELL F-101A
AIRPLANE AT MACH NUMBERS FROM 0.82 TO 1.84

By Earl C. Hastings, Jr., and Grady L. Mitcham

Langley Aeronautical Laboratory
Langley Field, Va.

CLASSIFIED DOCUMENT

This document contains classified information affecting the National Defense of the United States within the meaning of the Espionage Act, USC 18:793 and 794. Its transmission or the revelation of its contents in any manner to an unauthorized person is prohibited by law.

NATIONAL ADVISORY COMMITTEE FOR AERONAUTICS

WASHINGTON

~~CONFIDENTIAL~~
UNCLASSIFIED



NATIONAL ADVISORY COMMITTEE FOR AERONAUTICS

RESEARCH MEMORANDUM CLASSIFICATION CHANGED

for the

U. S. Air Force ~~CONFIDENTIAL~~

FLIGHT DETERMINATION OF THE *By authority of O-STAR Date 11-30-70*
V. 8, No. 22 *Blm*
12/22/70

LONGITUDINAL STABILITY AND CONTROL CHARACTERISTICS OF A
0.125-SCALE ROCKET-BOOSTED MODEL OF THE MCDONNELL F-101A

AIRPLANE AT MACH NUMBERS FROM 0.82 TO 1.84

By Earl C. Hastings, Jr., and Grady L. Mitcham

SUMMARY

A flight test has been conducted to determine the longitudinal stability and control characteristics of a 0.125-scale model of the McDonnell F-101A airplane for the Mach number range between 0.82 and 1.84.

The variation of lift-curve slope with Mach number was gradual with a maximum value of 0.107 occurring at a Mach number of 0.95.

The minimum drag coefficient (including base and internal drag) has a value of 0.020 at a Mach number of 0.87. The drag rise begins at a Mach number of 0.90, and at Mach number of 1.10 the minimum drag is 0.070. Above this Mach number there is a gradual increase in minimum drag coefficient to a value of 0.074 when the Mach number is 1.83.

The aerodynamic-center location moved from a value of 62 percent mean aerodynamic chord at a Mach number of 0.88 to its most rearward position of 85 percent at a Mach number of 1.40.

The all-movable horizontal tail remained an effective control for producing lift and pitching moment with the variation in effectiveness being gradual throughout the Mach number range covered by the test. There were no large or abrupt losses in pitch damping over the Mach number range covered.

UNCLASSIFIED
~~CONFIDENTIAL~~

5092

INTRODUCTION

A rocket-model program is being conducted by the Langley Pilotless Aircraft Research Division to determine some of the longitudinal and lateral stability derivatives of the McDonnell F-101A airplane at supersonic speeds. These tests are being conducted at the request of the U. S. Air Force. The McDonnell F-101A is designed to be a high-speed, long-range, fighter bomber powered by two Pratt and Whitney J-57 turbojet engines. The wing has a swept plan form with a leading-edge sweep-back angle of 41.12° . Longitudinal control is provided by an all-movable horizontal tail of aspect ratio 3.30 which is mounted high on the vertical fin. Conventional ailerons and rudder provide roll and directional control.

This paper presents longitudinal-stability, control-effectiveness, and drag data obtained from the flight of a 0.125-scale rocket-boosted model of the F-101A airplane between Mach numbers of 0.82 and 1.84. In addition to the longitudinal-stability and drag data presented herein, control-effectiveness and hinge-moment data are also included.

SYMBOLS

| | |
|---------------|---|
| A | cross-sectional area, sq ft |
| a_l/g | longitudinal-accelerometer reading |
| a_n/g | normal-accelerometer reading |
| b | wing span, ft |
| \bar{c} | mean aerodynamic chord, ft |
| C_C | chord-force coefficient, positive in a rearward direction, $\frac{a_l}{g} \frac{W}{S_w} \frac{l}{q}$ |
| C_D | drag coefficient, $C_N \sin \alpha + C_C \cos \alpha$ |
| C_{Db} | base drag coefficient, $\frac{-(p_{base} - p_o) \text{ base area}}{qS_w}$ |
| $C_{D_{min}}$ | minimum drag coefficient |

| | |
|---|--|
| C_h | hinge-moment coefficient, $\frac{\text{Hinge moment}}{q S_t \bar{c}_t}$ |
| C_L | lift coefficient, $C_N \cos \alpha - C_D \sin \alpha$ |
| $C_{L C_{D \min}}$ | lift coefficient for minimum drag |
| w | mass flow through duct, slugs/sec |
| w_0 | mass of air flowing through a stream tube of area equal to the inlet-cowl area under free-stream conditions, slugs/sec |
| M | Mach number |
| P_{base} | average base static pressure, lb/sq ft |
| P_0 | free-stream static pressure, lb/sq ft |
| P | period of short-period oscillation, sec |
| q | dynamic pressure, lb/sq ft |
| R | Reynolds number based on wing mean aerodynamic chord |
| C_m | pitching-moment coefficient about center of gravity |
| C_{m_0} | pitching-moment coefficient about center of gravity at zero angle of attack and horizontal-tail deflection |
| $C_{m_q} = \frac{\partial C_m}{\partial \left(\frac{\dot{\theta} \bar{c}}{2V} \right)}$ | per radian |
| $C_{m_{\dot{\alpha}}} = \frac{\partial C_m}{\partial \left(\frac{\dot{\alpha} \bar{c}}{2V} \right)}$ | per radian |
| $C_{m_q} + C_{m_{\dot{\alpha}}}$ | pitch-damping derivative |
| C_N | normal-force coefficient, positive toward top of model from model center line, $\frac{a_n}{g} \frac{W}{S_w} \frac{1}{q}$ |
| g | acceleration due to gravity, 32.2 ft/sec ² |

| | |
|--|---|
| I_y | moment of inertia about pitch axis, slug-ft ² |
| l | length, ft |
| r | radius of equivalent body of revolution, ft |
| S | area including intercept, sq ft |
| $t_{1/2}$ | time to damp to one-half amplitude, sec |
| V | velocity, ft/sec |
| W | weight of model, lb |
| x | station (measured from nose), ft |
| α | angle of attack of model center line, deg |
| $\dot{\alpha} = \frac{1}{57.3} \frac{d\alpha}{dt}$ | |
| γ | flight-path angle, measured with respect to a horizontal plane, radians |
| δ | horizontal-tail deflection, positive trailing edge down, deg |
| θ | angle between fuselage center line and horizontal, radians |
| Subscripts: | |
| w | wing |
| t | tail |

Derivatives are expressed in this manner: $C_{L_\alpha} = \frac{\partial C_L}{\partial \alpha}$; $C_{h_\delta} = \frac{\partial C_h}{\partial \delta}$; and so forth. A dot over a symbol indicates the first derivative with respect to time, and two dots indicate the second derivative with respect to time.

MODEL AND APPARATUS

Model

Figure 1 is a three-view drawing of the model tested in this investigation, and the physical characteristics of the model are given in

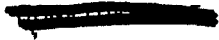


table I. The area distribution and equivalent body of revolution are shown in figure 2. This information is included for pressure-drag correlation at a Mach number of 1.0. A photograph of the model is shown as figure 3.

The model tested in this investigation had a pulsed horizontal tail and internal flow. Construction of the model was primarily of steel and duralumin plates and bulkheads with wooden fairings and plastic hatches forming the contoured body lines.

Both the wing and horizontal tail had swept plan forms. The wing thickness varied from 6.67 percent chord at the root to 5.71 percent chord at the tip. The airfoil sections were NACA airfoils modified by extending the chord 5 percent forward of the 16.04-percent-chord line and adding 1.67-percent positive camber. There was 1° of positive incidence between the wing and the model center line but there was no aileron deflection built into the wing. Duralumin plates and mahogany fillers comprised the wing panels, and stall plates were located at about 70 percent of each semispan.

The horizontal tail was solid duralumin and operated in abrupt movements between angles of approximately -1° and -5°. Operation of the tail was achieved by a hydraulically actuated piston. A motor-driven cam operating an electric solenoid was used to control the flow of the hydraulic fluid to the piston to insure proper timing of the pulsing operation.

The wing root inlet was unswept and incorporated a boundary-layer bleed. Internal ducting consisted of two separate ducts running through the model with a minimum cross section near each duct exit. A total-pressure rake was mounted slightly forward of this minimum section to obtain data to be used in the calculation of internal drag at supersonic Mach numbers. A fairing was installed in each duct in order to duplicate the location and cross-sectional area of the engines and accessory housings. The internal ducting did not duplicate that of the full-scale airplane; however, the exit-to-entrance area ratio was such as to regulate the mass flow to approximate the engine requirements at supersonic speeds. Since the afterburner base of the model did not duplicate that of the full-scale airplane, it was necessary to determine the base drag of the model. Six manifolded static-pressure tubes were used to determine the average static-pressure variation over the flat base of one of the afterburners.

The model contained no sustainer rocket motor and was boosted to Mach numbers near 2.0 by a 2.5-DS-59000 rocket motor. After the booster had stopped thrusting, the model separated from the booster and the data presented herein were obtained during this coasting phase of the flight. The booster-adaptor and drag-flap combination used in this test were modified on the basis of data obtained from tests of this configuration in the Langley 4- by 4-foot supersonic pressure tunnel (ref. 1). Figure 4 is a photograph of the model-booster combination prior to launching.

Apparatus

The model was instrumented with a telemeter system which measured longitudinal-stability and drag data during the flight and transmitted it to a ground receiving station. In addition to these primary data, other channels of information measured for analysis were angles of attack and sideslip, free-stream total pressure, model base pressure and duct total pressure, transverse acceleration and horizontal-tail deflection and hinge moment. A photograph of a typical telemeter installation and pulse system can be found in reference 2.

A radiosonde released at the time of firing recorded free-stream temperature and static pressure. The velocity of the model and its position in space were determined by a CW Doppler radar set and NACA modified radar tracking unit.

ANALYSIS OF DATA

Free oscillations of the model were created by pulsing the horizontal tail in an approximate square-wave motion which resulted in changes in normal acceleration, angle of attack, and hinge moment. The longitudinal stability analysis of these oscillations is based on two degrees of freedom in pitch. In the appendixes of references 2 and 3 can be found a more detailed discussion of the methods used in reducing the data from a flight time history to the parameters presented in this paper and the assumptions made in and the limits of the test technique.

Some of the control characteristics and damping data obtained from this test are incomplete between Mach numbers of 0.80 and 1.07 because the conditions of damped oscillations and linear variation of aerodynamic forces and moments with angle of attack discussed in reference 3 are not satisfied in this speed range. Values of these quantities in the speed range where they are incomplete were of secondary interest in this test. The primary data desired (longitudinal stability and drag) are complete over the entire test Mach number range.

The recorded values of angle of attack were corrected for instrument position error and tail position was corrected for tail bending due to high hinge moments in exactly the same manner as in reference 2. All coefficients, with the exception of hinge moments (which were based on the total horizontal-tail area), were computed based on the theoretical wing area (fillet area excluded), and all angles were measured relative to the model center line.

The total pitching-moment coefficients were calculated and corrected for aerodynamic damping by the following equation:

$$C_m = \frac{I_Y \ddot{\theta}}{q S_w \bar{c}_w} - \left[(C_{mq} + C_{m\dot{\alpha}}) \dot{\alpha} \right] \frac{\bar{c}}{2V} - (C_{mq} \dot{\gamma}) \frac{\bar{c}}{2V}$$

The angular acceleration in pitch was obtained from the following equation:

$$\ddot{\theta} = \frac{d\dot{\theta}}{dt} = \frac{d(\dot{\gamma} + \dot{\alpha})}{dt}$$

The quantity $\dot{\alpha}$ was obtained by differentiating the measured α curve and the quantity $\dot{\gamma}$ was calculated from the measured accelerations at the model center of gravity, the gravity component being neglected.

A choking section and a total-pressure rake installed in the duct exit made it possible to determine mass-flow ratio and internal drag based on free-stream and duct exit conditions (see ref. 4). The internal drag presented herein was calculated by the following equation:

$$C_{D_{\text{internal}}} = \frac{1}{q S_w} \left[w(V - V_{\text{exit}}) - A_{\text{exit}}(P_{\text{exit}} - P_0) \right]$$

ACCURACY

As discussed in reference 3 the possible error due to telemeter-instrument accuracy is generally proportional to the total calibrated instrument range. Quantities such as C_D and C_L are subject to the most error because they depend on measured accelerations, the dynamic pressure, and angle of attack.

For this test, Mach number was available between $M = 1.5$ and 1.84 from both Doppler radar and measured free-stream total pressure, whereas below $M = 1.5$ only free-stream total pressure was available. Agreement between the two sources from $M = 1.5$ to 1.84 was better than 1 percent; however, since only the free-stream total-pressure measurements were available below $M = 1.5$, the Mach number probably becomes less accurate as the Mach number decreases. Since the dynamic pressure is proportional to the Mach number squared, its probable inaccuracy throughout the speed range should be approximately twice that of the Mach number.

Some quantities whose accuracy varies with Mach number are tabulated for Mach numbers of 0.80 and 1.70 in the following table. Although these values of accuracy were predicted from the instrument ranges, the probable error due to this source may be less than the values presented in the table. It should be pointed out, however, that these errors are systematic rather than random.

| M | ΔC_L | ΔC_D |
|------|--------------|--------------|
| 0.80 | 0.060 | 0.005 |
| 1.70 | .020 | .002 |

The errors in the measured values of angles of attack and horizontal-tail deflection would be constant throughout the Mach number range of this test, since they are independent of dynamic pressure or velocity. The recorded tail deflections should be accurate to about 0.1° and angle of attack to about 0.3° .

Base- and internal-drag data were obtained from pressure measurements and therefore have different possible errors than the drag values based on acceleration measurements listed in the table. The maximum possible errors in both of these quantities due to instrument inaccuracy would be so small that they would not change any of the three-decimal-place drag values quoted herein.

RESULTS AND DISCUSSION

The Reynolds number range is shown as a function of Mach number in figure 5. Over this Mach number range the mass-flow ratio was a value of approximately 0.7. The maximum angles of sideslip encountered between $M = 0.86$ and 1.84 were of the order of $\pm 2.0^\circ$, whereas the average value was less than 1.0° .

Lift

Some representative plots of the variation of C_L with angle of attack are given in figure 6(a) and the lift-curve slope $C_{L\alpha}$ taken over the linear portion of these plots is presented in figure 6(b) as a function of Mach number.

No nonlinearity was present below $C_L = 0.50$. The lift-curve slope varies from a value of 0.102 at $M = 0.82$ to a maximum value of 0.107 at $M = 0.95$, followed by a gradual decrease to a value of 0.057 at $M = 1.79$. Also presented for comparison in figure 6 are some unpublished wind-tunnel values of $C_{L\alpha}$ obtained over the same lift range as the values presented from this test. The tunnel data presented at $M = 1.20$ and below are from the Wright Air Development Center 10-foot transonic tunnel and those at $M = 1.55$ and $M = 1.90$ are from tests at the Ames 6- by 6-foot supersonic tunnel. The agreement between these sources of data and the present test is considered good.

Buffet.- The flight time history of normal acceleration showed the presence of high-frequency oscillations as the model pitched to the higher lift coefficients below $M = 0.95$. These oscillations are believed to represent the buffet-intensity rise, which occurred at about $C_L = 0.59$ at $M = 0.93$ and $C_L = 0.65$ at $M = 0.86$ with the maximum amplitude being $\Delta C_L \approx 0.1$. As a result of the high frequency of the oscillations (115 cps) and since obtaining buffet information was not a primary purpose of this test, the minimum amplitude of ΔC_L which can be obtained from the instrumentation used is 0.03.

Drag

The basic drag data for the 0.125-scale model of the McDonnell F-101A airplane are presented in the form of lift-drag curves in figure 7. These curves are for various Mach numbers and lift ranges and the drag values include both internal and base drag.

Minimum drag.- The variations of the lift coefficient for minimum drag $C_{L_{C_{Dmin}}}$ and the minimum drag coefficient C_{Dmin} as determined from the lift-drag curves of figure 7 are presented as a function of Mach number in figures 8 and 9. The values of C_{Dmin} include both internal and base drag. Values of $C_{Dinternal}$ and C_{Dbase} are also presented in figure 9. At the higher horizontal-tail deflections the model did not oscillate to minimum drag.

Between $M = 0.82$ and $M = 0.87$, C_D is constant at about 0.020. The drag rise occurs at $M = 0.90$ (the Mach number at which $\frac{dC_D}{dM} = 0.10$) and at $M = 1.10$, C_D has a value of 0.070. The drag continues to increase gradually with Mach number and at $M = 1.83$ has a value of $C_D = 0.074$.

Base drag.- Also shown in figure 9 are the base drag data obtained from the base pressure survey. The base drag coefficient varied from about 0.001 at subsonic speeds to about 0.002 at supersonic speeds.

Internal drag.- The values of internal-drag coefficient shown in figure 9 are a nearly constant value of 0.005 from $M = 1.01$ to $M = 1.84$. No subsonic values could be obtained since the duct became unchoked below $M = 1.0$, but other tests have shown that the internal-drag level remains about the same at subsonic and supersonic speeds.

Static Longitudinal Stability

The static longitudinal stability characteristics of the model are shown in figures 10 and 11. All moment data were taken about the center of gravity at $0.169\bar{c}$.

The curves presented in figure 10(a) show pitching-moment coefficient C_m against C_L for various tail deflections at Mach numbers equal to or greater than 1.0 and figure 10(b) shows pitching-moment curves at Mach numbers less than 1.0.

At Mach numbers above 1.09 the curves presented in figure 10(a) are linear for the C_L range covered but at $M = 1.09$ there is a change in pitching-moment slope at $C_L = 0.05$.

Figure 10(b) shows that at $M = 0.94$ and $M = 0.95$ there is a change in the slope of the pitching-moment curves beginning at $C_L = 0.10$. The curve at $M = 0.85$ shows the variation of C_m with C_L in the lift range from $C_L = 0.56$ to the stall at $C_L = 0.83$. The curve shows non-linearity above $C_L = 0.74$.

The values of aerodynamic center shown in figure 11 were determined from the slopes of the pitching-moment curves in the lift range where they were linear. At $M = 0.94$ and $M = 0.95$ the values of aerodynamic center were determined only at lift coefficients greater than 0.10.

Another check on the value of aerodynamic center was made by using the period of the short-period longitudinal oscillation resulting from the control movement (fig. 12) and the time to damp to half amplitude (fig. 13). These quantities were used to calculate the longitudinal-stability parameter $C_{m\alpha}$ by the following relation:

$$C_{m\alpha} = \frac{-I_Y}{qS_w \bar{c}_w} \left[\frac{4\pi^2}{P^2} + \left(\frac{0.693}{t_{1/2}} \right)^2 \right]$$

These values of $C_{m\alpha}$ in conjunction with $C_{L\alpha}$ were used to compute aerodynamic-center values for comparison with those obtained from the pitching-moment curve and are shown in figure 11.

The aerodynamic center moved from a location of 62 percent mean aerodynamic chord at $M = 0.88$ to its most rearward location of 85 percent mean aerodynamic chord at about $M = 1.40$ and then decreased to a value of 81 percent mean aerodynamic chord at $M = 1.72$. Values of aerodynamic center as determined from the two sources of unpublished wind-tunnel data are plotted for comparison in figure 11.

Damping in Pitch

The damping-in-pitch characteristics of the model are given by the parameters $t_{1/2}$ and $C_{m_q} + C_{m\dot{\alpha}}$ which are presented in figures 13 and 14, respectively. These parameters were determined from an analysis of the rate of decay of the transient short-period oscillations resulting from abrupt horizontal-tail movements. Figure 14 shows a decrease in pitch damping between $M = 0.90$ and 1.02 followed by a gradual increase to $M = 1.40$ and a more rapid increase between $M = 1.40$ and $M = 1.75$. Pitch-damping data from the rocket test of a model having a horizontal tail of aspect ratio 4.33 (ref. 5) show the same general variation of $C_{m_q} + C_{m\dot{\alpha}}$ with Mach number. The model tested in this investigation showed no large variation or abrupt loss in damping through the speed range presented.

The horizontal stabilizer, however, did not remain at a fixed angle but oscillated about a mean trim line in phase with α as a result of the high hinge moments at supersonic speeds. The maximum $\Delta\delta$ of this oscillation was in the order of 0.5° with an average value of about 0.25° . The static derivatives were corrected for this effect; however, no dynamic corrections were made for this effect.

Longitudinal Control Effectiveness

The effectiveness of the all-movable aspect-ratio-3.30 horizontal tail in producing lift and pitching moments is given in figures 15 and 16. The lift coefficient per degree of tail deflection $C_{L\delta}$ has a value of 0.0105 at about $M = 1.05$ and decreases gradually with increase in Mach number until at $M = 1.70$ the value of $C_{L\delta}$ is 0.0070. Unpublished estimates of $C_{L\delta}$ made by the McDonnell Aircraft Corporation are plotted for comparison in figure 15. Agreement is generally good. Pitching-moment effectiveness $C_{m\delta}$ varies from -0.0362 at $M = 1.00$ to a value of -0.023 at $M = 1.70$.

Two other longitudinal control effectiveness parameters, the change in trim angle of attack per degree of tail deflection $\left(\frac{\Delta\alpha}{\Delta\delta}\right)_{\text{trim}}$ and the rate of change in trim lift coefficient with tail deflection $\frac{\Delta C_{L_{\text{trim}}}}{\Delta\delta}$, are presented as functions of Mach number in figures 17 and 18.

The horizontal tail is an effective pitch control throughout the Mach number range presented and all of the effectiveness parameters shown in figures 15 to 18 show gradual variations with Mach number.

Longitudinal Trim

The basic pitching-moment coefficient C_{m_0} at zero tail deflection and zero angle of attack is shown in figure 19. The wing of the model had 1° of positive incidence relative to the model center line, which was used as the reference in this test. Since most of the tunnel data used the wing as the reference, figure 19 shows C_{m_0} computed using $\alpha = 0^\circ$ relative to the wing as well as the model center line. Unpublished wind-tunnel data are plotted for comparison and the agreement is good at supersonic speeds. A value of C_{m_0} was computed at $M = 0.88$ by using rocket-model values of $C_{m_{C_L}}$ and $C_{L_{\alpha}}$ and unpublished wind-tunnel values of control effectiveness. The agreement between this value of C_{m_0} and the tunnel value at $M = 0.90$ is good.

Values of C_{m_0} calculated for 0° wing angle of attack vary from 0.078 at $M = 1.06$ to 0.048 at $M = 1.77$.

Hinge Moments

The hinge-moment characteristics of the horizontal tail in the form of the variation of hinge-moment coefficient with angle of attack C_{h_α} and the variation of hinge-moment coefficient with tail deflection C_{h_δ} are given in figures 20 and 21. The parameter C_{h_α} was obtained from the linear portion of plots of C_h against α (approximately 0° to 4°) and C_{h_δ} was determined by the method discussed in reference 2. The horizontal tail was hinged at 26.5 percent of the tail mean aerodynamic chord and had an unswept hinge line.

Figure 20 shows that $C_{h\alpha}$ varies from a value of 0.0020 at $M = 0.82$ to $C_{h\alpha} = -0.0075$ at $M = 1.55$ and at $M = 1.72$ has a value of -0.0055 . Figure 21 shows a steady decrease in $C_{h\delta}$ from -0.0170 at $M = 1.07$ to $C_{h\delta} = -0.0073$ at $M = 1.70$.

CONCLUSIONS

Results from the flight test of a 0.125-scale model of the McDonnell F-101A airplane from Mach number 0.82 to Mach number 1.84 indicate the following conclusions:

1. Lift-curve slope varies gradually with Mach number, a maximum value of 0.107 occurring at a Mach number of 0.95 then decreasing gradually with increasing Mach number to a value of 0.057 at a Mach number of 1.79.
2. The minimum drag coefficient (including base and internal drag) has a value of 0.020 at a Mach number of 0.87. The drag rise begins at a Mach number of 0.90, and at Mach number of 1.10 the minimum drag is 0.070. Above this Mach number there is a gradual increase in minimum drag to a value of 0.074 when the Mach number is 1.83.
3. There is no nonlinearity in the supersonic pitching-moment curves above Mach number 1.09 for the lift-coefficient range covered. At Mach numbers of 0.94 and 0.95 there is a change in pitching-moment slope at a lift coefficient of 0.10.
4. The aerodynamic-center location has a value of 62.0 percent mean aerodynamic chord at a Mach number of 0.88 and reaches its most rearward position of 85.0 percent mean aerodynamic chord at a Mach number of 1.40.
5. The pitch-damping parameters indicated that the model possessed dynamic longitudinal stability throughout the speed range, though there is a decrease in damping between Mach numbers of 0.90 and 1.02.
6. Variation of horizontal-tail effectiveness with Mach number from 1.00 to 1.70 was gradual and the tail remained an effective control for producing forces and moments throughout the speed range.

7. The pitching-moment coefficient at 0° wing angle of attack and 0° tail deflection decreases from a positive value of 0.078 at a Mach number of 1.06 to 0.048 at a Mach number of 1.77.

Langley Aeronautical Laboratory,
National Advisory Committee for Aeronautics,
Langley Field, Va., June 17, 1955.

Earl C. Hastings, Jr.

Earl C. Hastings, Jr.
Aeronautical Research Scientist

Grady L. Mitcham
Grady L. Mitcham
Aeronautical Engineer *by E.C.H.*

Approved:

P. R. Hill
for

Joseph A. Shortal
Chief of Pilotless Aircraft Research Division

rmw

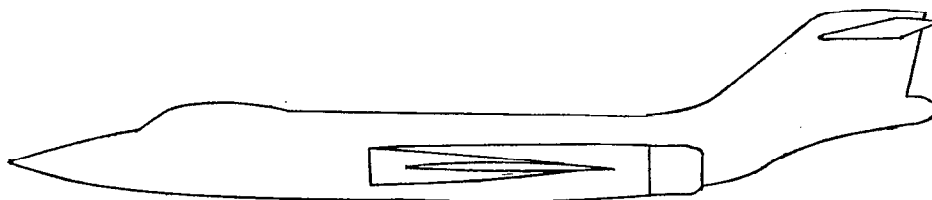
REFERENCES

1. Robinson, Ross B.: Effects of Free-Flight Rocket-Model Booster-Adapter Configurations on the Aerodynamic Characteristics in Pitch and Sideslip of a Swept-Wing Fighter Airplane Model at a Mach Number of 2.01. NACA RM L55B01, 1955.
2. Mitcham, Grady L., Stevens, Joseph E., and Norris, Harry P.: Aerodynamic Characteristics and Flying Qualities of a Tailless Triangular-Wing Airplane Configuration As Obtained From Flights of Rocket-Propelled Models at Transonic and Low Supersonic Speeds. NACA RM L9L07, 1950.
3. Gillis, Clarence L., Peck, Robert F., and Vitale, A. James: Preliminary Results From a Free-Flight Investigation at Transonic and Supersonic Speeds of the Longitudinal Stability and Control Characteristics of an Airplane Configuration With a Thin Straight Wing of Aspect Ratio 3. NACA RM L9K25a, 1950.
4. Faget, Maxime A., Watson, Raymond S., and Bartlett, Walter A., Jr.: Free-Jet Tests of a 6.5-Inch-Diameter Ram-Jet Engine at Mach Numbers of 1.81 and 2.00. NACA RM L50L06, 1951.
5. Peck, Robert F., and Hollinger, James A.: A Rocket-Model Investigation of the Longitudinal Stability, Lift, and Drag Characteristics of the Douglas X-3 Configuration With Horizontal Tail of Aspect Ratio 4.33. NACA RM L53F19a, 1953.

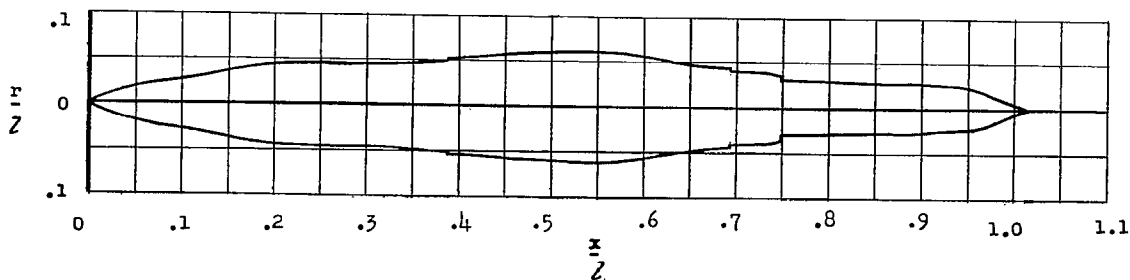
TABLE I
 PHYSICAL CHARACTERISTICS OF A 0.125-SCALE MODEL
 OF THE MCDONNELL F-101 AIRPLANE

| | |
|--|------------------|
| Wing: | |
| Area (theoretical), sq ft | 5.75 |
| Span, ft | 4.97 |
| Aspect ratio | 4.28 |
| Mean aerodynamic chord, ft | 1.28 |
| Taper ratio | 0.28 |
| Sweepback of leading edge, deg | 41.12 |
| Sweepback of trailing edge, deg | 19.42 |
| Incidence angle (with respect to model center line), deg | 1.0 |
| Dihedral angle, deg | 0.0 |
| *Root thickness (theoretical), percent chord | 6.67 |
| *Tip thickness, percent chord | 5.71 |
| Horizontal tail: | |
| Total area, sq ft | 1.17 |
| Span, ft | 1.97 |
| Aspect ratio | 3.30 |
| Mean aerodynamic chord, ft | 0.62 |
| Taper ratio | 0.46 |
| Sweepback of leading edge, deg | 39.80 |
| Sweepback of trailing edge, deg | 20.95 |
| Dihedral angle, deg | 10.0 |
| Hinge-line location, percent of tail mean aerodynamic chord | 26.5 |
| Root airfoil section | NACA 65A007 mod. |
| Tip airfoil section | NACA 65A006 mod. |
| Tail length (25 percent wing MAC to 25 percent tail MAC), ft | 3.69 |
| Fuselage: | |
| Length, ft | 8.38 |
| Width (maximum), ft | 0.96 |
| Height (maximum), ft | 0.88 |
| Maximum cross-sectional area, sq ft | 0.66 |
| Ducts (one side): | |
| Inlet area, sq ft | 0.0625 |
| Exit area, sq ft | 0.0474 |
| Area at compressor face (excluding area blocked by accessory housing), sq ft | 0.0802 |
| Vertical tail: | |
| Area above fuselage (dorsal excluded), sq ft | 1.18 |
| Span, ft | 0.94 |
| Mean aerodynamic chord (theoretical), ft | 1.46 |
| Aspect ratio (theoretical) | 0.66 |
| Sweepback angle at leading edge, deg | 52.00 |
| Sweepback angle at trailing edge, deg | 16.60 |
| Root airfoil section | NACA 65A007 |
| Tip airfoil section | NACA 65A007 |
| Weight and balance: | |
| Weight, lb | 405.25 |
| Wing loading, lb/sq ft | 70.5 |
| Center-of-gravity position, percent \bar{c} | 16.90 |
| Moment of inertia in pitch, slug-ft ² | 54.95 |

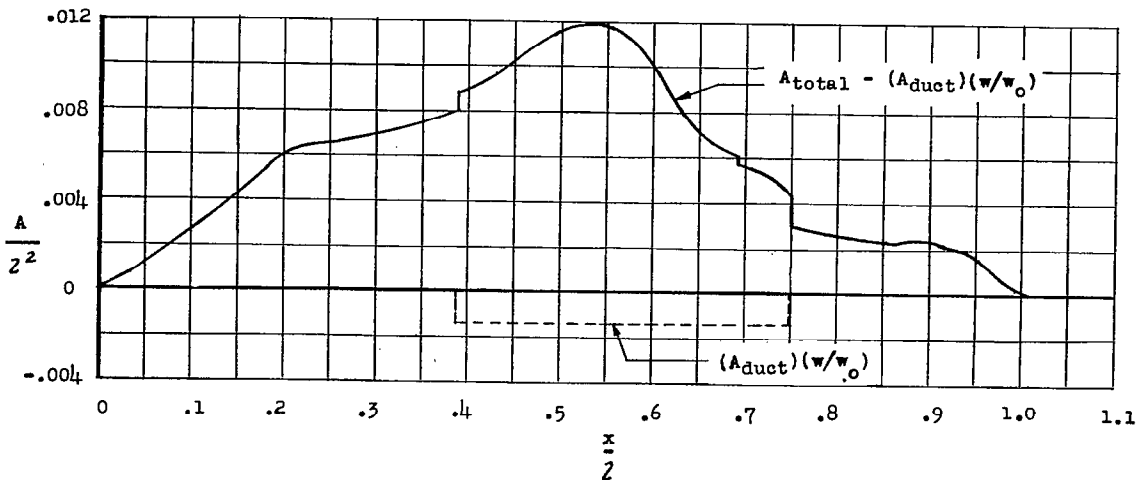
*Root and tip airfoil sections are NACA 65A007 and 65A006, respectively, modified by extending the chord 5 percent forward of the 16.04-percent-chord line and adding 1.67 percent positive camber.



Model



(a) Equivalent body of revolution.



(b) Area distribution.

Figure 2.- Area distribution and equivalent body of revolution of the model.

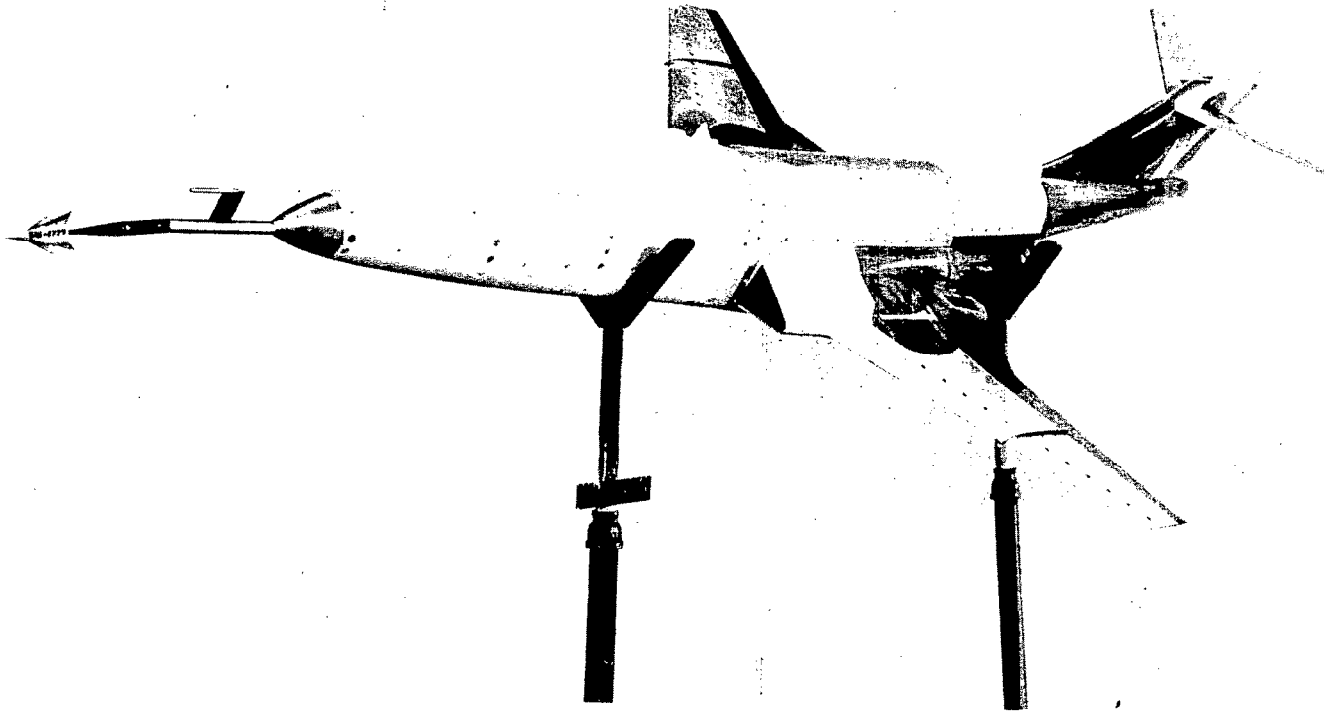


Figure 3.- Photograph of the model.

L-86586.1



Figure 4.- Booster-model combination on the launcher. L-86652.1

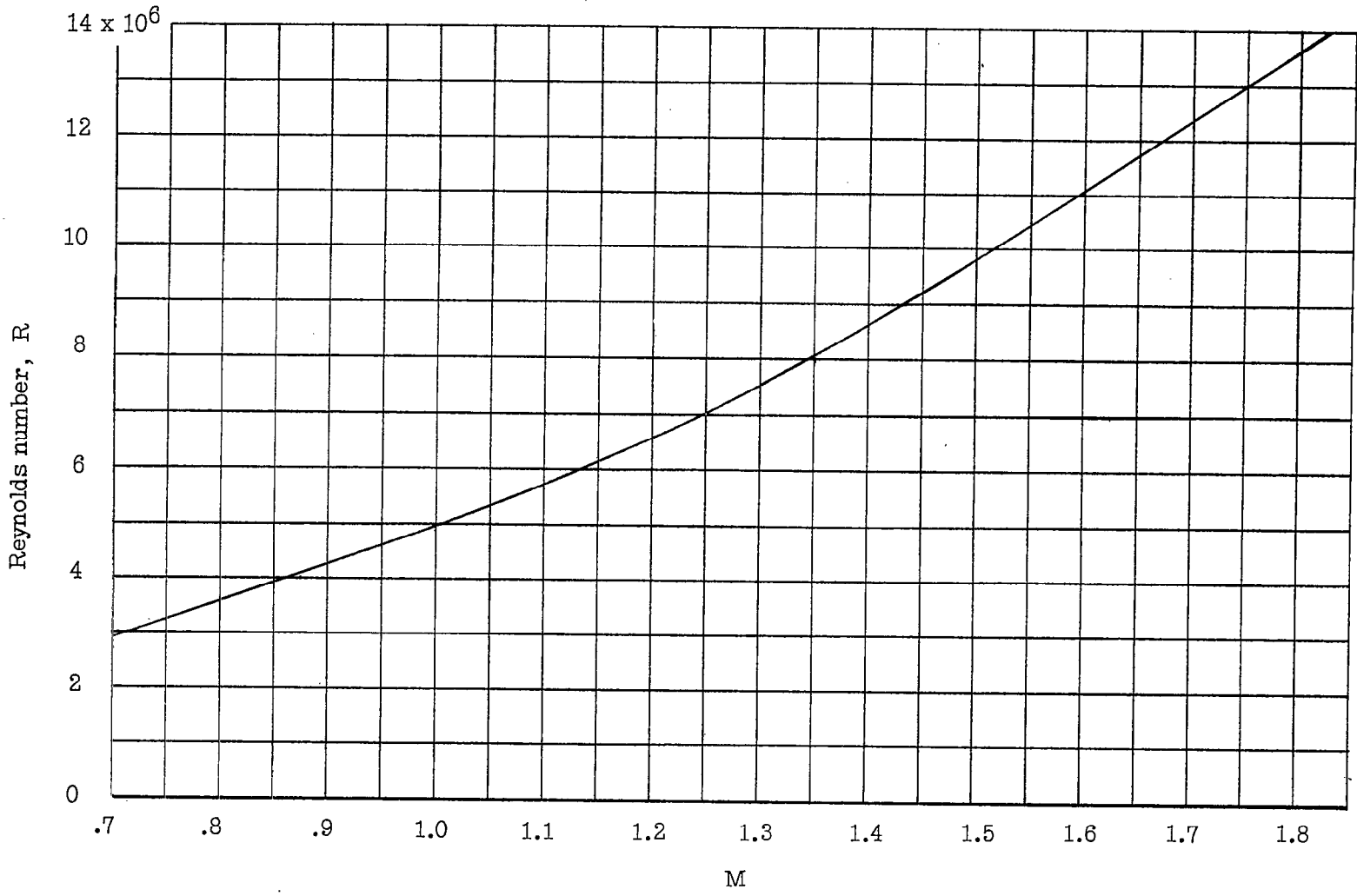
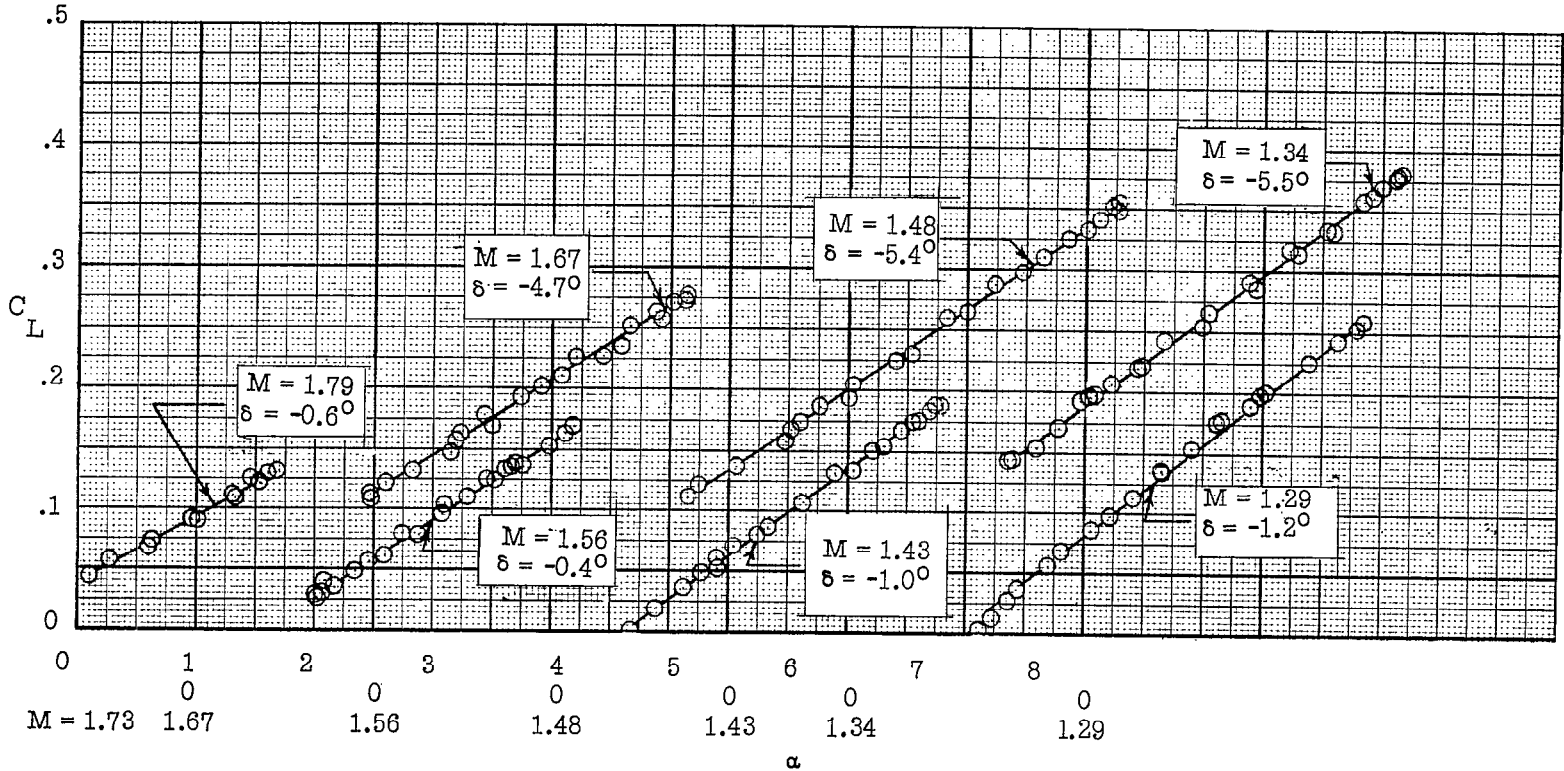


Figure 5.- Reynolds number as a function of Mach number.

CONFIDENTIAL

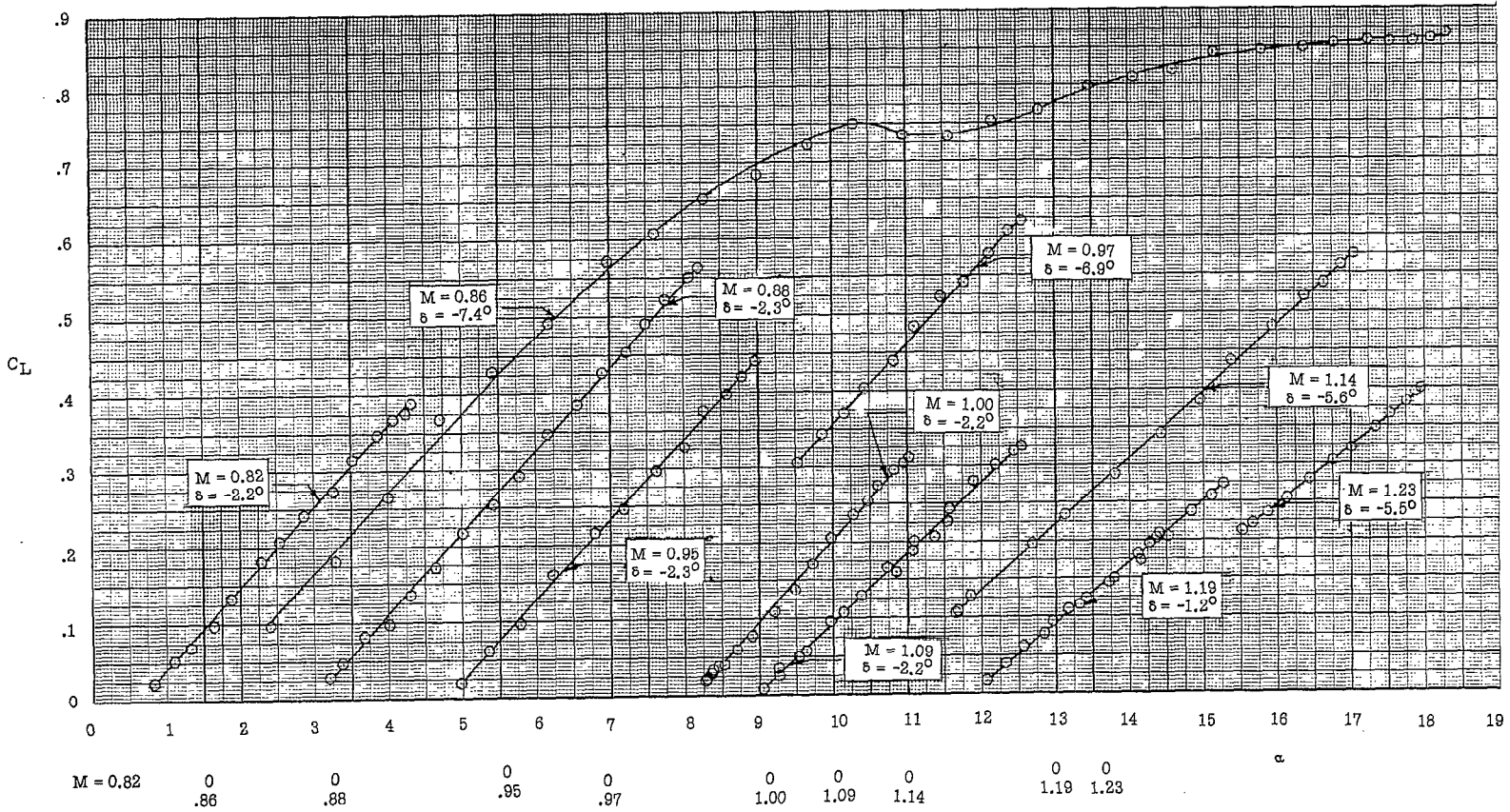


(a) Lift coefficient as a function of angle of attack.

Figure 6.- Lift characteristics of the model.

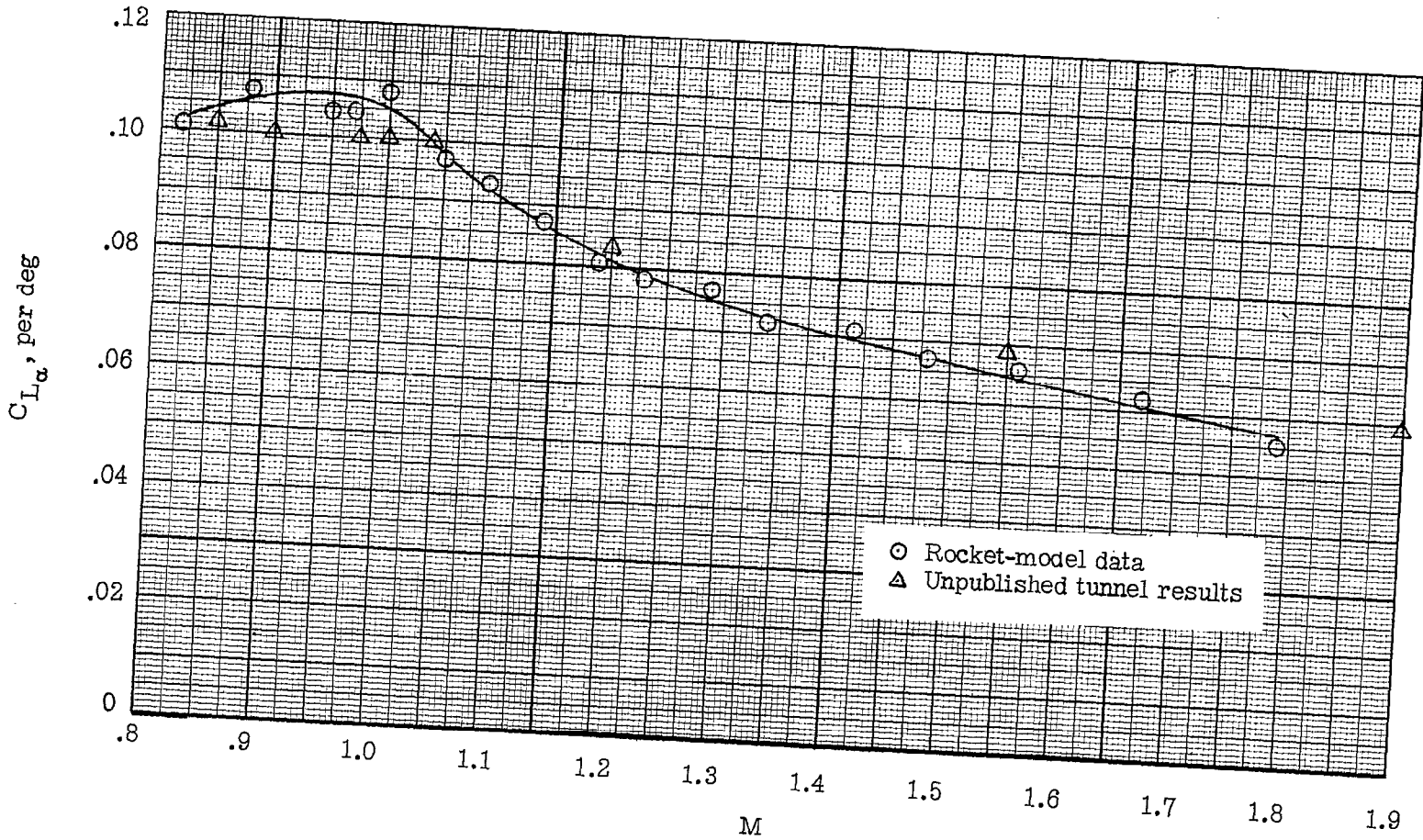
CONFIDENTIAL

CONFIDENTIAL



(a) Concluded.

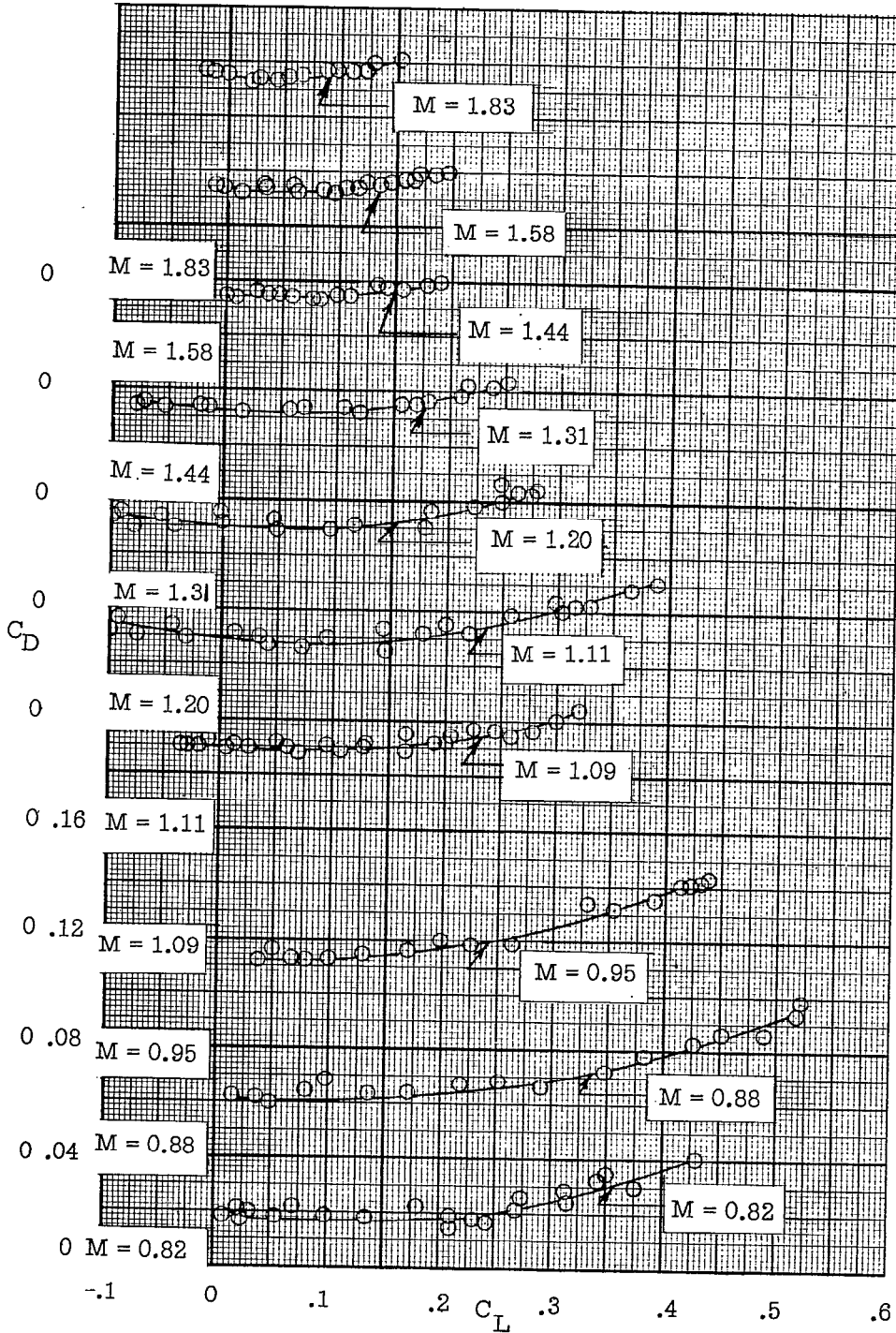
Figure 6.- Continued.



(b) Variation of lift-curve slope with Mach number.

Figure 6.- Concluded.

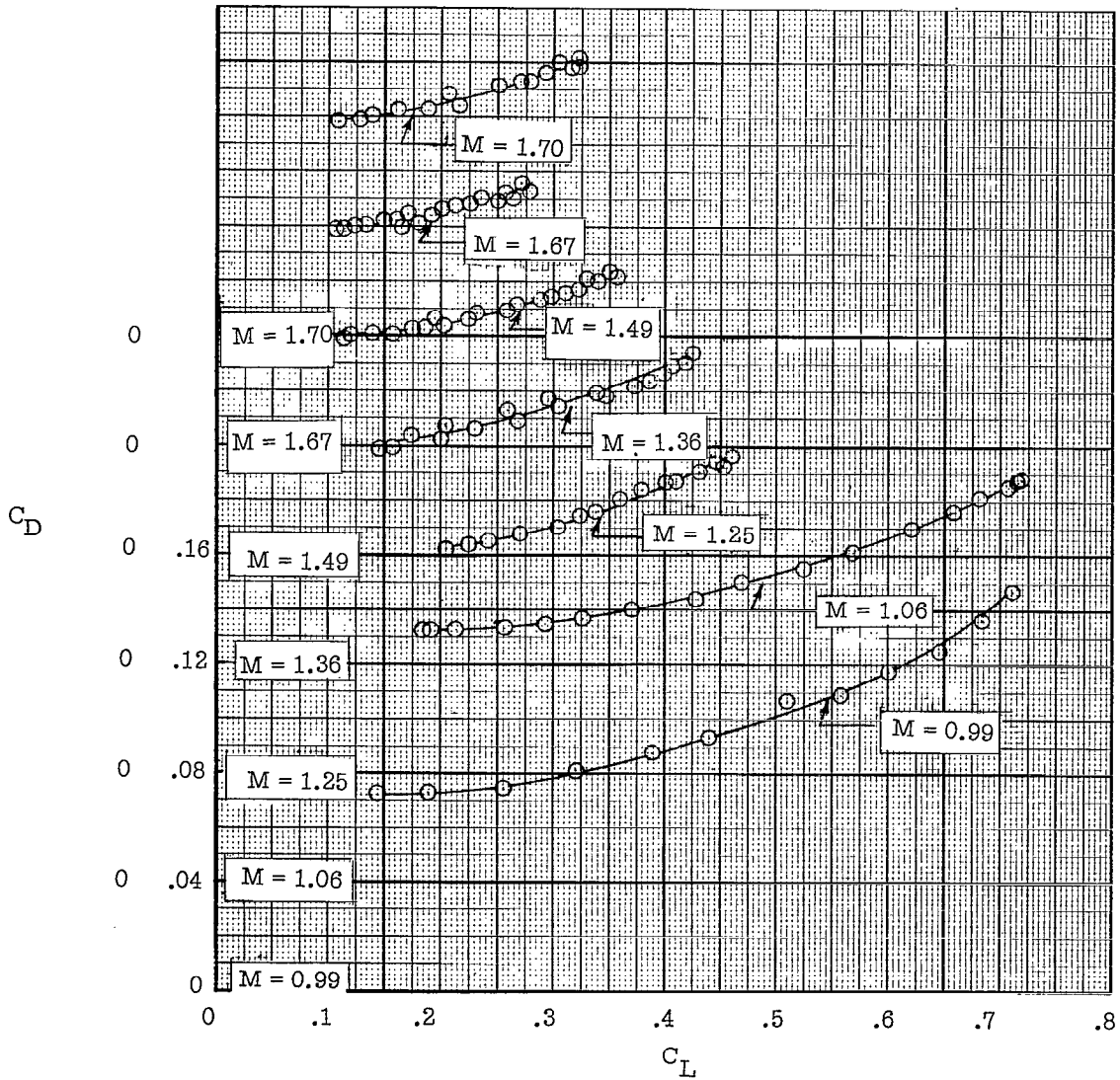
~~CONFIDENTIAL~~



(a) $\delta \approx -1.0^\circ$.

Figure 7.- Variation of drag coefficient with lift coefficient. Drag coefficient includes internal and base drag.

~~CONFIDENTIAL~~



(b) $\delta \approx -5.5^\circ$.

Figure 7.- Concluded.

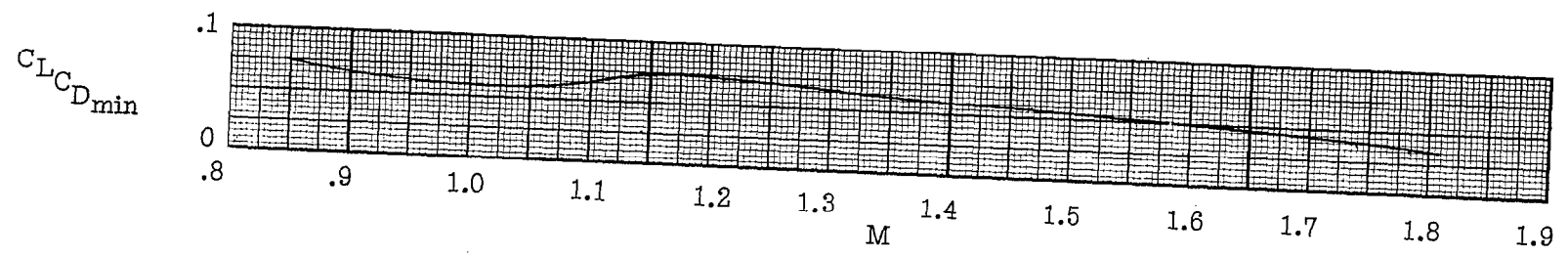


Figure 8.- Lift coefficient for minimum drag.

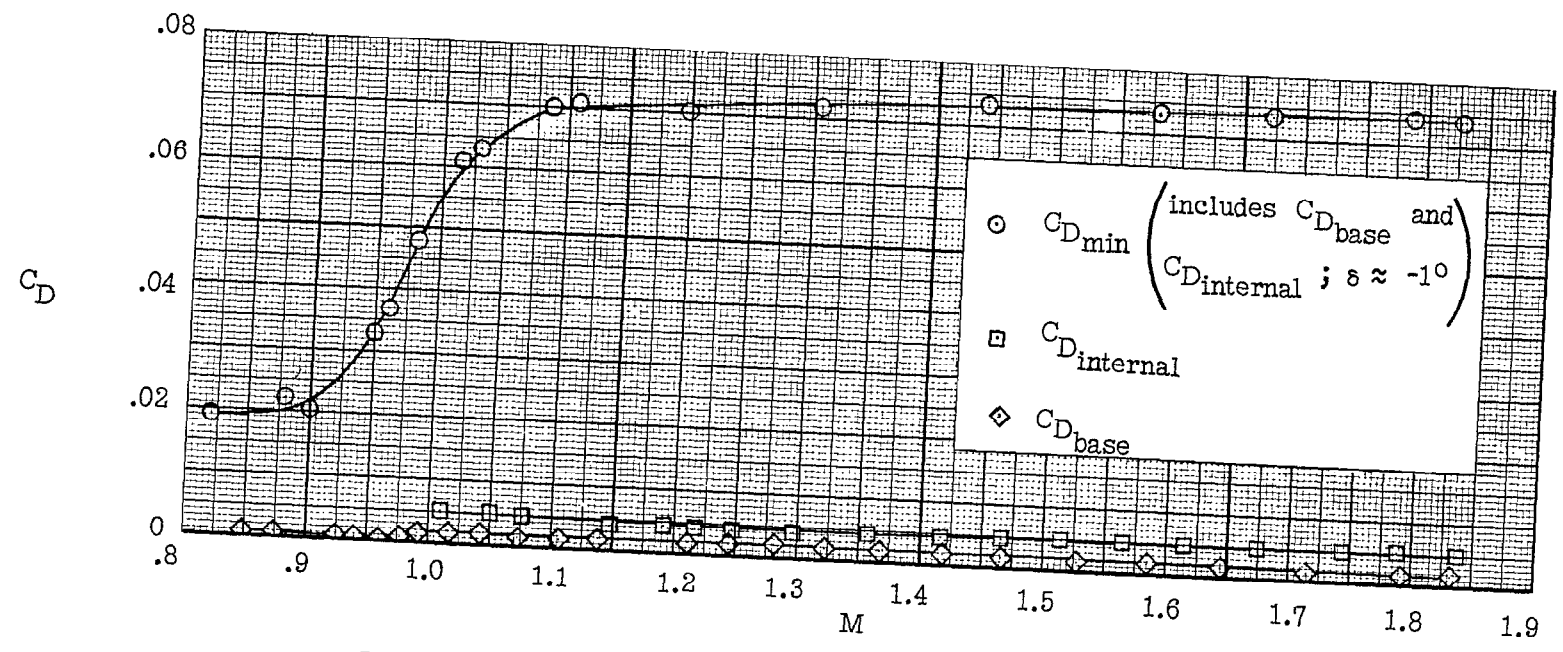
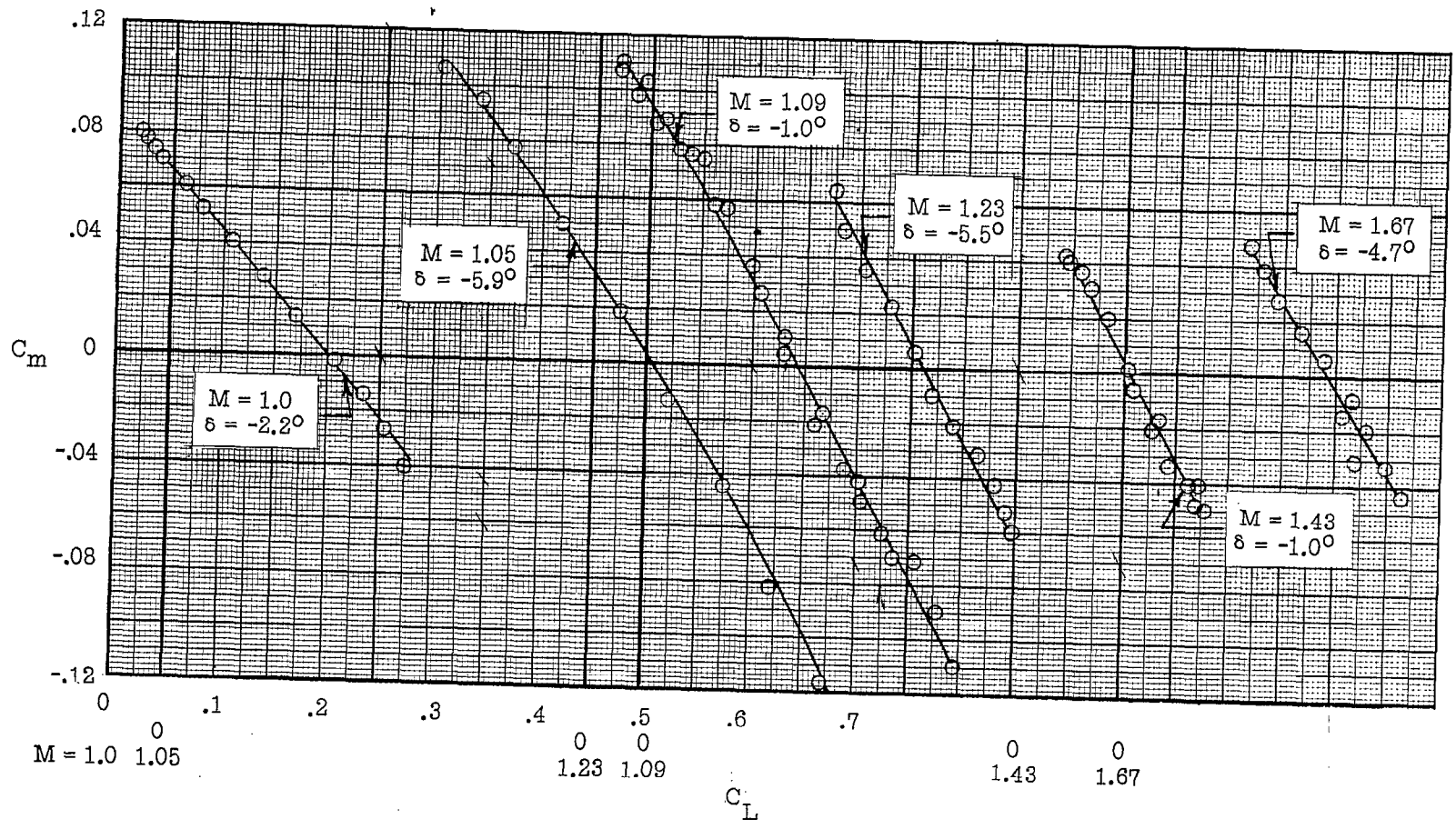


Figure 9.- Drag coefficient as a function of Mach number.

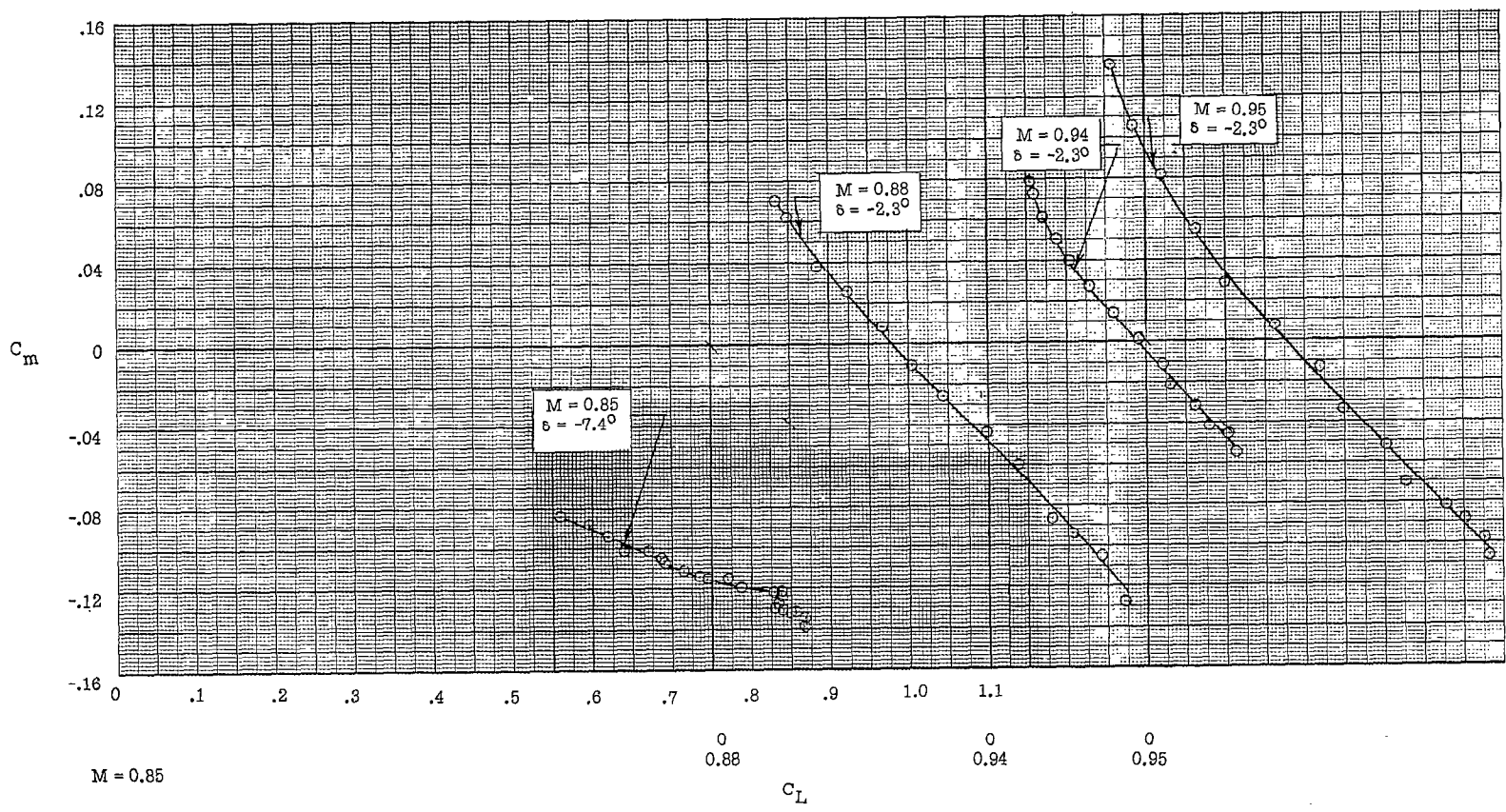
CONFIDENTIAL

CONFIDENTIAL



(a) $M \geq 1.0$.

Figure 10.- Variation of pitching-moment coefficient with lift coefficient. Center of gravity at $0.169\bar{c}$.



(b) $M < 1.0$.

Figure 10.- Concluded.

CONFIDENTIAL

CONFIDENTIAL

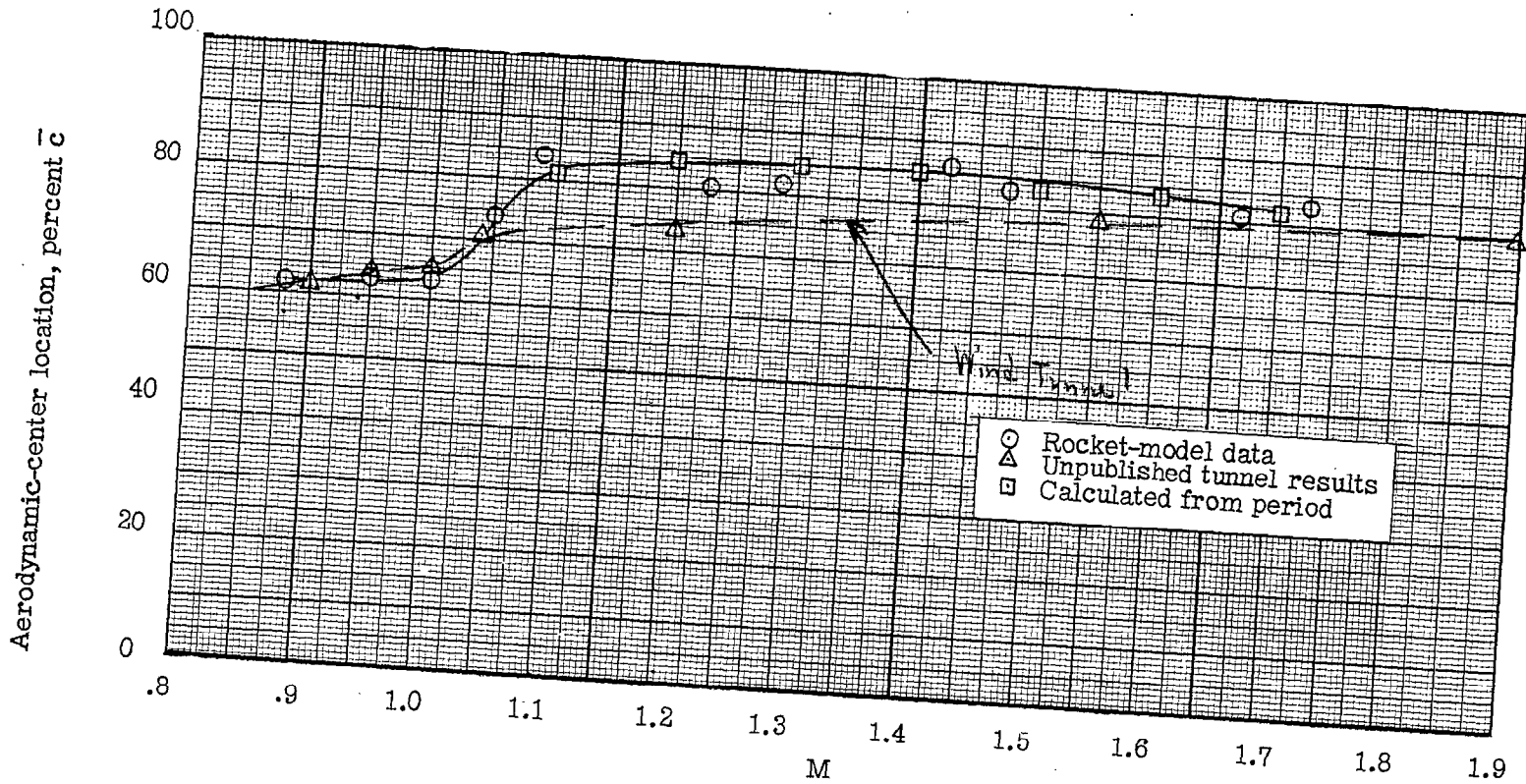


Figure 11.- Aerodynamic-center location.

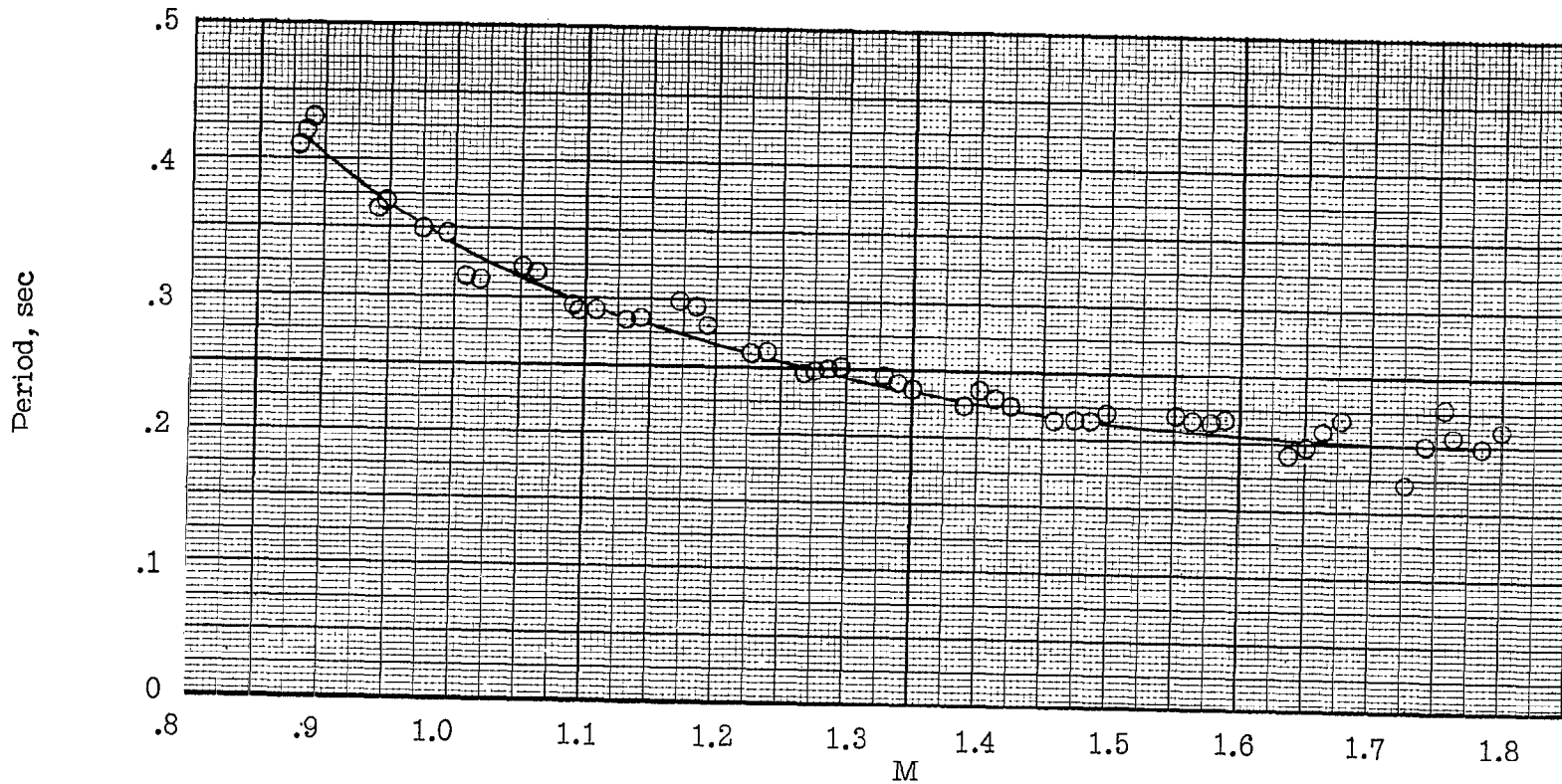


Figure 12.- Period of the longitudinal oscillation.

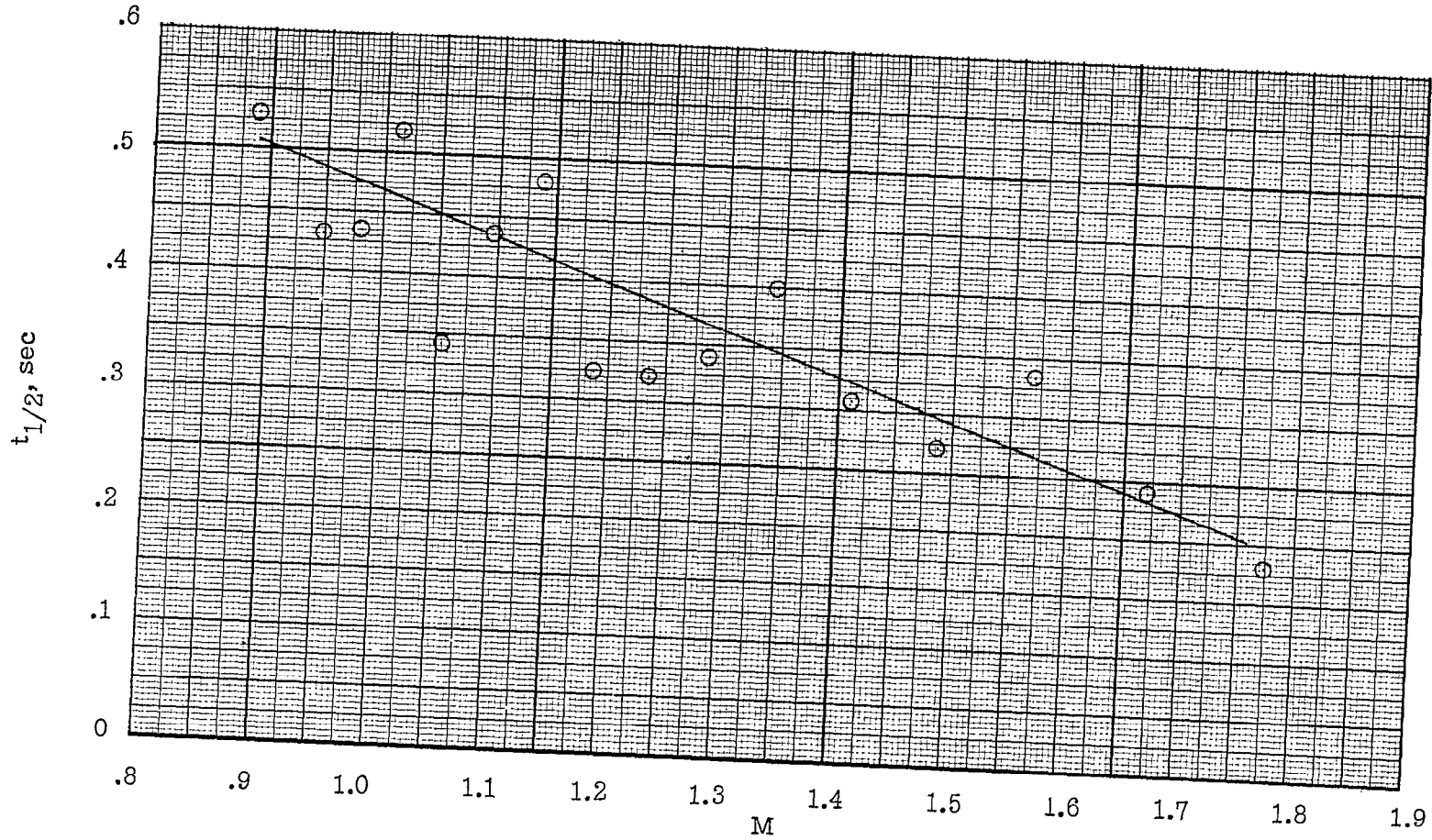


Figure 13.- Time to damp to half amplitude.

SECRET

~~CONFIDENTIAL~~

$C_{mq} + C_{m\dot{\alpha}}$, per radian

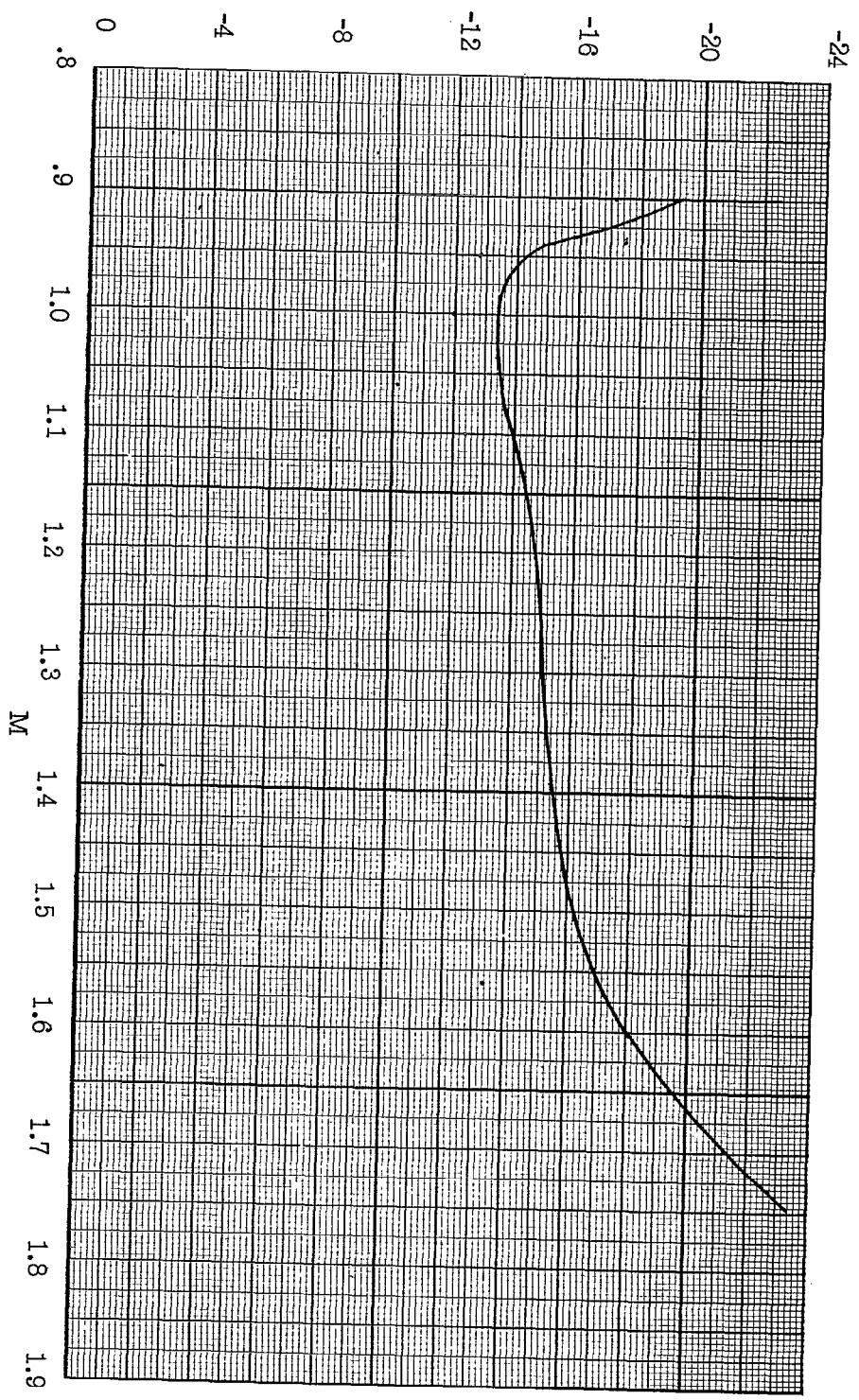


Figure 14.-- Pitch-damping parameter. Center of gravity at 0.169c.

~~CONFIDENTIAL~~

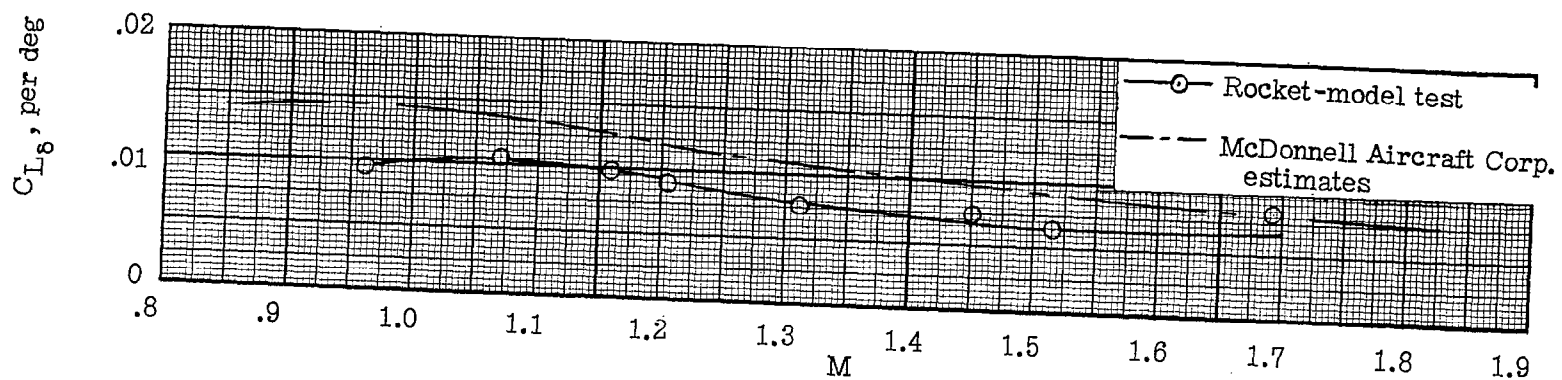
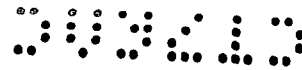


Figure 15.- Control lift effectiveness.

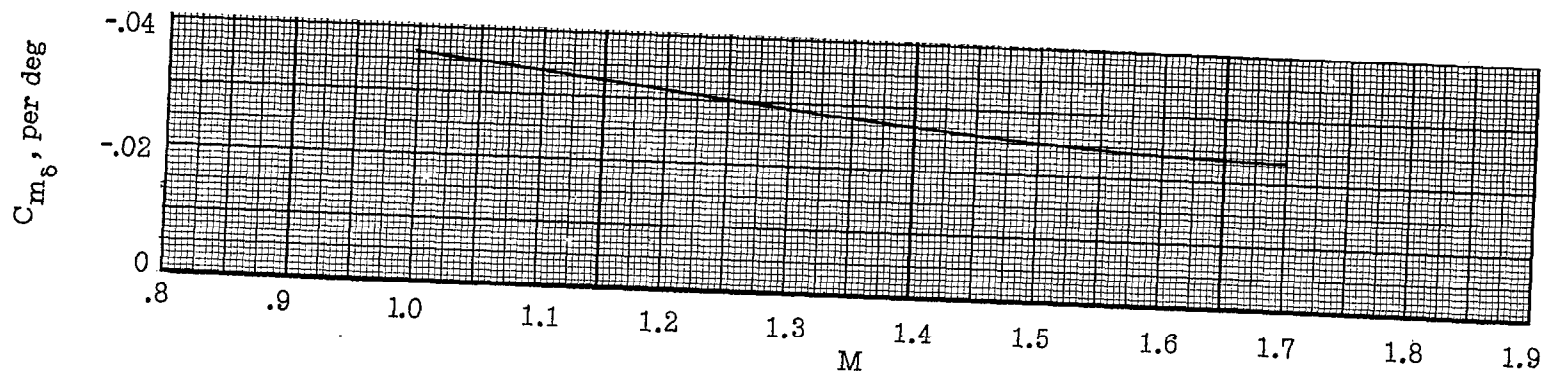


Figure 16.- Control pitching effectiveness. Center of gravity at 0.169c.

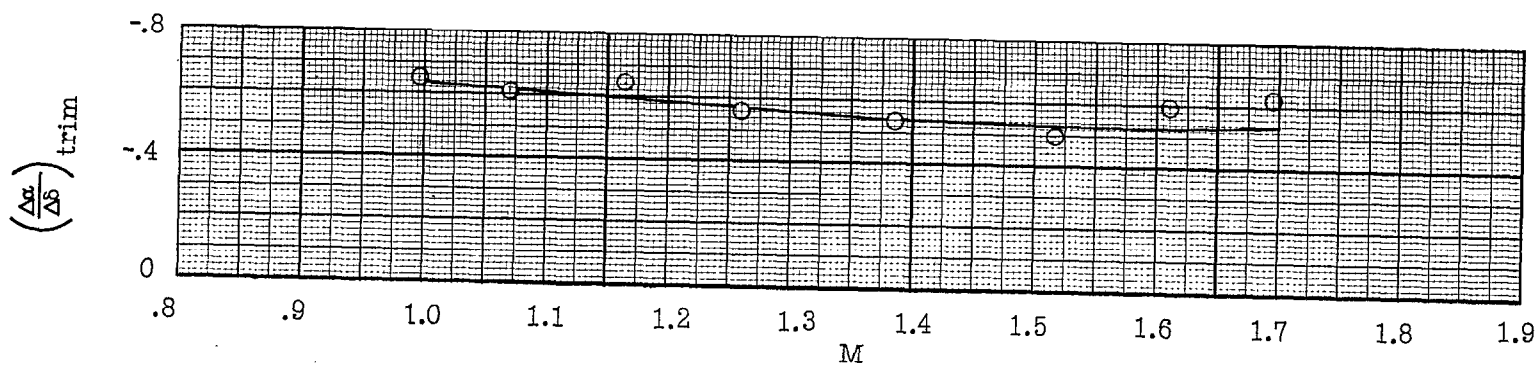


Figure 17.- Change in trim angle of attack per degree of tail deflection.

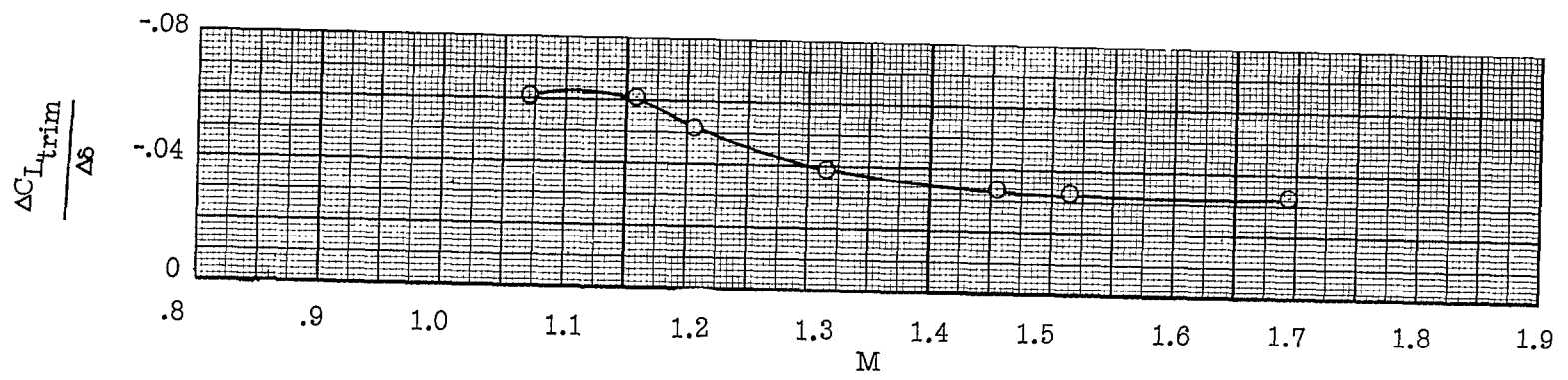


Figure 18.- Change in trim lift coefficient per degree of tail deflection.

CONFIDENTIAL

CONFIDENTIAL

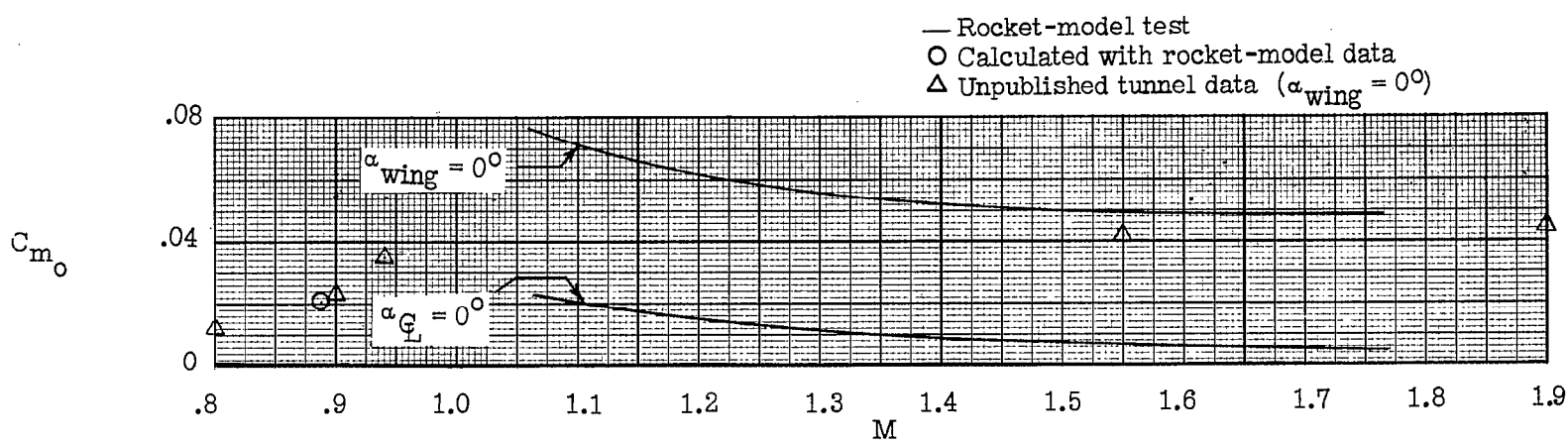
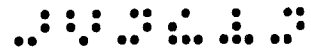


Figure 19.- Basic pitching-moment coefficient.



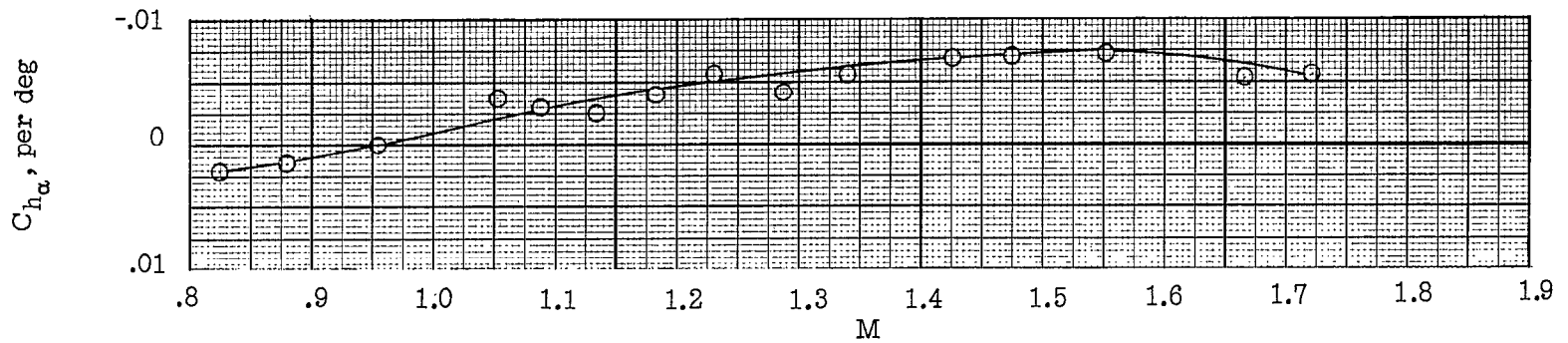
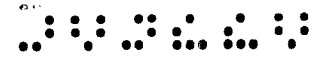


Figure 20.- Effect of Mach number on C_{h_α} .

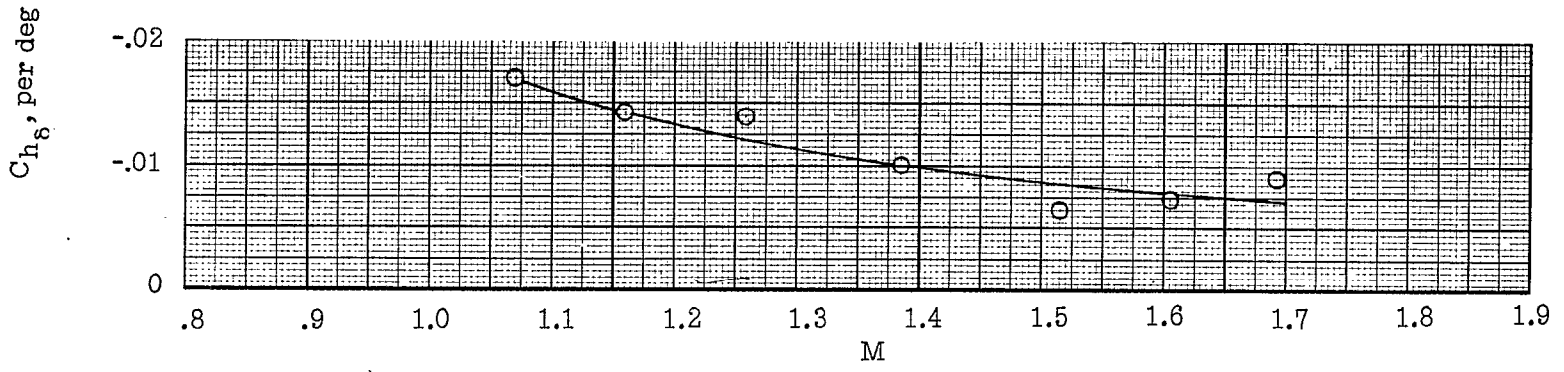


Figure 21.- Effect of Mach number on C_{h_δ} .

UNCLASSIFIED

UNCLASSIFIED